

1 **The importance of turbulent ocean-sea ice nutrient exchanges for**
2 **simulation of ice algal biomass and production with CICE6.1 and**
3 **Icepack 1.2**

4
5 Pedro Duarte¹, Philipp Assmy¹, Karley Campbell^{2,3}, Arild Sundfjord¹

6 ¹ Norwegian Polar Institute, Fram Centre, Tromsø, Norway

7 ² Department of Arctic and Marine Biology, UiT The Arctic University of Norway, Norway

8 ³ Bristol Glaciology Centre, University of Bristol, UK

9 *Correspondence to:* Pedro Duarte (Pedro.Duarte@npolar.no)

10 **Abstract.** Different sea-ice models apply unique approaches in the computation of nutrient diffusion between the ocean and
11 the ice bottom, which are generally decoupled from the calculation of turbulent heat flux. Often, a simple molecular diffusion
12 formulation is used. We argue that nutrient transfer from the ocean to sea ice should be as consistent as possible with heat
13 transfer, since all these fluxes respond to varying forcing in a similar fashion. We hypothesize that biogeochemical models
14 which do not consider such turbulent nutrient exchanges between the ocean and the sea-ice, despite considering brine drainage
15 and bulk exchanges through ice freezing/melting, may underestimate bottom-ice algal production. The Los Alamos Sea Ice
16 Model (CICE + Icepack) was used to test this hypothesis by comparing simulations without and with diffusion of nutrients
17 across sea-ice bottom dependent on velocity-shear, implemented in a way that is consistent with turbulent heat exchanges.
18 Simulation results support the hypothesis, showing a significant enhancement of ice algal production and biomass when
19 nutrient limitation was relieved by bottom-ice turbulent exchange. Our results emphasize the potentially critical role of
20 turbulent exchanges to sea ice algal blooms, and the importance of thus properly representing them in biogeochemical models.
21 The relevance of this becomes even more apparent considering ongoing trends in the Arctic Ocean, with a predictable shift
22 from light to nutrient limited growth of ice algae earlier in the spring, as the sea ice becomes more fractured and thinner with
23 a larger fraction of young ice with thin snow cover.

24 **1 Introduction**

25 Momentum, heat and mass fluxes between the ocean and the sea-ice are of utmost importance to predict sea-ice motion,
26 thermodynamics, and biogeochemistry. However, when we look at models released over the last decades, we find not only
27 inter-model differences in the physical concepts used to describe the processes responsible for some of the above fluxes, but
28 also intra-model differences in the approaches used in calculating, for example, heat and mass fluxes. In this work we will
29 focus on the differences related with the vertical diffusion of tracers between the water column and the bottom-ice and attempt
30 to explore their consequences on nutrient limitation for sea-ice algal growth.

31 We may divide the ocean-ice exchange processes into those related to: (i) entrapment during freezing; (ii) flushing and release
32 during melting; (iii) brine gravity drainage, driven by density instability, parameterized as either a diffusive or a convective
33 process; (iv) molecular diffusion; and (v) turbulent diffusion at the interface between the ocean and the ice induced by velocity
34 shear – the latter process being the focus of this study (e.g. Arrigo et al, 1993 and references therein; Jin et al., 2006; McPhee,
35 2008; Notz and Worster, 2009; Turner et al., 2013; Tedesco and Vichi, 2010, 2019; Jeffery et al., 2011; Vancoppenolle et al.,
36 2013).

37 These processes are considered in several sea ice models. Arrigo et al. (1993) distinguished nutrient exchanges resulting from
38 gravity drainage in brine channels, from brine convection in the skeletal layer, dependent on the ice growth rate. These brine
39 fluxes were used to calculate nutrient exchanges as a diffusive process. Lavoie et al. (2005) also calculated nutrient exchanges
40 as a diffusive process. Jin et al. (2006; 2008) computed nutrient fluxes across the bottom layer as an advection process
41 dependent on ice growth rate and based on Wakatsuchi and Ono (1983). Molecular diffusion was also considered. More
42 recently, other authors have integrated formulations of “enhanced diffusion” (Vancoppenolle et al., 2010; Jeffery et al., 2011)
43 or convection (Turner et al., 2013), based on hydrostatic instability of brine density profiles, to compute brine gravity drainage
44 and tracer exchange within the ice and between the ice and the sea water. Comparisons between salt dynamics in growing sea
45 ice with salinity measurements showed that convective Rayleigh number-based parameterizations (e.g. Wells et al., 2011),
46 such as the one by Turner et al. (2013), outperform diffusive and simple convective formulations (Thomas et al., 2020).

47 Interestingly, heat exchange is often calculated differently from salinity in models. In the case of the former, typically, a
48 transfer mechanism (turbulent or not) at the interface between the ocean and the sea ice is not dependent on any type of brine
49 exchange. In the case of salinity, such a mechanism is not considered (e.g. Vancoppenolle et al., 2007; Turner et al., 2013).
50 Presumably, such differences result from the relative importance of various physical processes for different tracers. Heat
51 transfer between the ice and the water is a fundamental mechanism in explaining sea-ice thermodynamics, irrespective of brine
52 exchanges. On the other hand, ice desalination depends mostly on brine gravity drainage and flushing during melting (Notz
53 and Worster, 2009).

54 Vertical convective mixing of nutrients under the sea ice may result from brine rejection and/or drainage from the sea ice (Lake
55 and Lewis, 1970; Niedrauer and Martin, 1979; Reeburgh, 1984) and from turbulence due to shear instabilities generated by
56 drag at the interface between the ocean and the sea ice (Gosselin et al., 1985; Cota et al., 1987; Carmack, 1986), internal waves
57 and topographical features (Ingram et al., 1989; Dalman et al., 2019). Gosselin et al. (1985) and Cota et al. (1987) stressed the
58 significance of tidally induced mixing in supplying nutrients to sympagic algae. Biological demand for silicic acid (hereafter
59 abbreviated as silicate) and nitrate is limited by the physical supply (Cota and Horne, 1989; Cota and Sullivan, 1990).

60 The analysis of several models published over the last decades and their approaches to calculate tracer diffusion across the ice-
61 ocean interface shows that some models do not consider this process or limit it to molecular diffusion. Other models consider
62 turbulent exchanges parameterized as a function of the Rayleigh number, calculated from brine vertical density gradients. Only
63 two of the sampled models (Lavoie et al., 2005 and Mortenson et al., 2017) use parameterizations based on friction velocity.
64 The former uses eddy diffusion to simulate the vertical supply of nutrients to the molecular sublayer, where nutrient fluxes

65 and their supply to the bottom ice are limited by molecular diffusion. The latter uses a coupled ocean-sea ice model but,
66 ultimately, molecular diffusion is the controlling process. Both authors use the same approach to compute the thickness of the
67 molecular sublayer, based on friction velocity.

68 In the absence of ice growth and when brine gravity drainage is limited, diffusive nutrient exchanges between the ocean and
69 the ice have the capacity to limit primary production. This limitation will be alleviated in the presence of a turbulent exchange
70 mechanism. We argue that nutrient transfer at the interface between the ocean and the sea ice should be as consistent as possible
71 with heat transfer since all these fluxes are closely linked. We hypothesize that models which do not consider the role of current
72 velocity shear on turbulent nutrient exchanges between the ocean and the sea-ice may underestimate bottom-ice algal
73 production.

74 To test the above hypothesis, we use a 1D vertically resolved model implemented with CICE+Icepack and contrast results
75 using the default diffusion parameterization and a “turbulent” parameterization analogous to that of heat and salt transfer, at
76 the interface between the ocean and the sea ice, based on McPhee (2008). This implementation of the turbulent
77 parameterization is specific for the software used and it may be different in other models.

78 **2 Methods**

79 **2.1 Concepts**

80 Turbulent exchanges may be parameterized through the flux of a quantity at the interface between the ocean and the sea ice,
81 calculated as the product of a scale velocity and the change in the quantity from the boundary to some reference level (McPhee,
82 2008):

$$83 \langle w' S' \rangle = \alpha_s u^* (S_w - S_0) \quad (1)$$

84 Where, $\langle w' S' \rangle$ represents the averaged co-variance of the turbulent fluctuations of interface vertical velocity (m s^{-1}) and
85 salinity, respectively, α_s is an interface salt/nutrient exchange coefficient (dimensionless); u^* is the friction velocity (m s^{-1}); S_0
86 and S_w are interface and far-field salinities, respectively.

87 We calculate nutrient exchanges using a similar approach:

$$88 F_N = -\alpha_s u^* (N_w - N_0) \quad (2)$$

89 This is an extension of the concept used for heat and salt by McPhee (2008) (see page 112, Fig. 6.3). The minus sign used in
90 (2) is for compatibility with the CiCE + Icepack convention that upward fluxes are negative (e.g. Hunke et al., 2015). α_s varies
91 between $8.6 \cdot 10^{-5}$, during the melting season, and 0.006, during winter (McPhee et al., 2008).

92 Before explaining how 3 was implemented in the CICE+Icepack we describe the model vertical biogeochemical grid (biogrid),
93 the tracer equation and the bottom boundary conditions. The biogrid is the non-dimensional grid used for discretizing the
94 vertical transport equations of biogeochemical tracers, defined between the brine height (h), which takes the value zero, and

95 the ice-ocean interface, which takes the value one (Jeffery et al., 2016). The Icepack tracer equation (without biogeochemical
 96 reaction terms for the sake of simplicity) may be written as [for more details, refer Jeffery et al. (2011; 2016)]:

$$97 \quad \varphi \frac{\partial N}{\partial t} = \left\{ \frac{(x-1)}{h} \frac{\partial z_t}{\partial t} - \frac{x}{h} \frac{\partial z_b}{\partial t} \right\} \frac{\partial}{\partial x} (\varphi N) + \frac{1}{h} \frac{\partial}{\partial x} (w_f N) + \frac{\partial}{\partial x} \left(\frac{D_{MLD} + \varphi D_m}{h^2} \frac{\partial N}{\partial x} \right) \quad (3)$$

98 Where $0 \leq x \leq 1$ is the relative depth of the vertical domain of the biogrid, z_t and z_b are vertical positions of the ice top and
 99 bottom (m), respectively, φ is sea ice porosity, w_f is the Darcy velocity due to the sea ice flushing of tracers (m s^{-1}), D_m is the
 100 molecular diffusion coefficient and D_{MLD} is the mixed length diffusion coefficient ($\text{m}^2 \text{s}^{-1}$). D_{MLD} is detailed in Jeffery et al.
 101 (2011) and it is zero when the brine vertical density gradient is stable, otherwise (when density increases towards the ice top)
 102 it is calculated as:

$$103 \quad D_{MLD} = \frac{gk}{\mu} \Delta \rho_e l \quad (4)$$

104 Where g is the acceleration of gravity (9.8 m s^{-2}), k is sea ice permeability ($2.2 \text{ kg m}^{-1}\text{s}^{-1}$), μ is dynamic viscosity ($2.2 \text{ kg m}^{-1}\text{s}^{-1}$), ρ_e is the
 105 equilibrium brine density and l is a length scale (7 m). The values shown here are the default ones in CICE+Icepack.

106 The bottom boundary condition of 3 is based on values of N at the sea ice bottom interface (N_0 at $x=1$) and in the ocean (N_w)
 107 (Jeffery et al., 2011), Therefore, the last term of equation 3 at the bottom boundary may be written as:

$$108 \quad \frac{D_{MLD} + \varphi D_m}{h^2 \partial x} (N_0 - N_w) \quad (5) \text{With}$$

109 With $\varphi=1$.

110 In CICE+Icepack, diffusion time scales are calculated separately for later usage in 3 as:

$$111 \quad \tau = \frac{D_m}{h^2} [\text{s}^{-1}] \quad (6)$$

112 And

$$113 \quad \tau = \frac{D_{MLD}}{h^2} [\text{s}^{-1}] \quad (7)$$

114 A similar timescale for the turbulent process described by equation 3 may be calculated from:

$$115 \quad \tau = \frac{\alpha_s u^*}{h} [\text{s}^{-1}] \quad (8)$$

116 Therefore, in the Los Alamos Sea Ice Model the implementation of turbulent diffusion nutrient exchanges at the ice-ocean
 117 interface is quite straightforward. In other models, other approaches may be required.

118 The usage of h in these timescales implies merely the way they are normalized in the code before the actual diffusive fluxes
 119 are calculated considering the distance between the points ($h \cdot \partial x$, see above equation 3) where variables are calculated, along
 120 the layers of the biogrid. The product $h \cdot x$ corresponds to the actual distance of a given point from the top of the biogrid.

121 In the simulations using turbulent diffusion, we perform the same calculations, except that the molecular diffusion term $\frac{\varphi D_m}{h^2}$
 122 is replaced with a turbulent diffusion term $\frac{\alpha_s u^*}{h}$ at the interface between the last model layer and the ocean. This exchange
 123 process takes place “outside” the sea ice where $\varphi=1$, affecting directly only the tracer concentration at the ice-ocean interface.

125 From equations 6 - 8 it turns out that the product $\alpha_s u$ by distance (z) has the same dimensions of D_m or D_{MLD} , corresponding to
126 a turbulent diffusion coefficient. Assuming $z \approx 0.01$ m, turbulent diffusion induced by velocity shear becomes comparable with
127 molecular diffusion only for $u^* < 0.0012$ m s $^{-1}$, considering the lower end of the α_s range ($8.6 \cdot 10^{-5}$, see above) or $u^* < 1.7 \cdot 10^{-5}$
128 m s $^{-1}$, considering the upper end of the α_s range (0.006). If we assume instead $z \approx 0.00054$ m [the average thickness of the
129 molecular sublayer reported in Lavoie et al. (2005)], the calculated u^* values increase by one-two orders of magnitude
130 (depending on α_s) but are still low (0.0004-0.03 m s $^{-1}$). In fact, such low friction velocities would require low “stream”
131 velocities - relative ice-ocean velocities. For an account of the relationship between “stream” and friction velocities under the
132 sea ice see Supplementary information 3 of Olsen et al. (2019) and references therein. These authors show that “stream”
133 velocities of only a few centimetres per second lead to friction velocities one order of magnitude lower but still in the order of
134 0.001 ms $^{-1}$, i.e., larger only than the highest u^* values estimated above. Considering current velocities relative to the sea ice
135 observed during the N-ICE2015 cruise [Granskog et al., 2018; Figure 2d of Duarte et al. (2017)], with most values between
136 0.05 and > 0.2 m s $^{-1}$, it is rather likely that friction velocities under the ice are frequently above the thresholds calculated above
137 and that turbulent diffusion will dominate over molecular diffusion. Dalman et al. (2019) provided experimental evidence for
138 such turbulent nutrient fluxes to the ice bottom, leading to increased chlorophyll concentrations at the bottom ice, in a strait
139 with strong tidal currents. The mechanism treated here as turbulent diffusion seems analogous to “forced convection” in the
140 lowermost parts of the brine network, which is driven by pressure differences caused by the shear under the sea ice (Neufeld,
141 2008; Vancoppenolle et al., 2013).

142 2.2 Implementation

143 We used the Los Alamos Sea Ice Model, which is managed by the CICE Consortium with an active forum
144 (<https://bb.cgd.ucar.edu/cesm/forums/cice-consortium.146/>) and a git repository (<https://github.com/CICE-Consortium>). It
145 includes two independent packages: CICE and Icepack. The former computes ice dynamic processes and the latter ice column
146 physics and biogeochemistry. Their development is handled independently with respect to the GitHub repositories
147 (<https://github.com/CICE-Consortium>). All the changes described below were implemented in two forks to the above
148 repository, one for Icepack and another for CICE and they may be found in Duarte (2021a and b, respectively).

149 Our simulations may be run using only Icepack, since they are focused on ice column physics and biogeochemistry, without
150 the need to consider ice dynamic processes. However, we used both CICE + Icepack together to allow for use of netCDF based
151 input/output not included in Icepack. Therefore, we defined a 1D vertically resolved model with 1 snow layer and 15 ice layers
152 and 5X5 horizontal cells. This is the minimum number of cells allowable in CICE due to the need to include halo cells (only
153 the central “column” is simulated). Therefore, ice column physics and biogeochemistry were calculated by Icepack but CICE
154 was the model driver. The input file (ice_in) used in this study was included in our CICE fork and it lists all parameters used
155 in the model and described in Hunke et al. (2016), Jeffery et al. (2016), Duarte et al. (2017) and in Tables S1 and S2. Any
156 changes in “default” parameters or any other model settings will be specified.

157 We made several modifications in CICE to allow using forcing time series collected during the Norwegian young sea ice (N-
158 ICE2015) expedition (Granskog et al., 2018) and described in Duarte et al. (2017) (see Fig. 2 of the cited authors). These
159 modifications were meant to allow reading of forcing data at higher frequencies than possible with the standard input
160 subroutines in the CICE file ice_forcing.F90.

161 When the dynamical component of CICE is not used, u^* is set to a minimum value instead of being calculated as a function of
162 ice-ocean shear stress (Hunke et al., 2015). Duarte et al. (2017) implemented shear calculations from surface current velocities
163 (one of the models forcing functions) irrespective of the use of the CICE dynamics code. These modifications were also
164 incorporated in the current model configuration so that shear can be used to calculate friction velocity and, thereafter, influence
165 heat and tracer/nutrient exchanges, following Eqs. (1) and (8) and parameters described in McPhee et al. (2008). When the
166 parameter kdyn is set to zero in ice_in, ice dynamics is not computed, but shear is calculated in the modified subroutine
167 icepack_step_therm1, file icepack_therm_vertical.F90. If kdyn is not zero, these calculations are ignored since shear is already
168 calculated in the dynamical part of the CICE code.

169 A Boolean parameter (Bottom_turb_mix) was added to the input file, which is set to “false” or “true” when the standard
170 molecular diffusion approach or the new turbulent based diffusion approach is used, respectively. Another Boolean parameter
171 (Limiting_factors_file) was added to the ice_in file. When set to “true” limiting factor values for light, temperature, nitrogen,
172 and silicate are written to a text file every model timestep. These are calculated by Icepack biogeochemistry, according to
173 Jeffery et al. (2016), but there is no writing-output option in the standard code.

174 **2.3 Model simulations**

175 Simulations were run for a refrozen lead (RL) without snow cover and for second-year sea ice (SYI) with ~40 cm snow cover
176 monitored in April-June during the N-ICE2015 expedition (Granskog et al., 2018 and Fig. 1 of Duarte et al. 2017). Details on
177 model forcing with atmospheric and oceanographic data collected during the N-ICE2015 expedition, including citations and
178 links to the publicly available datasets are given in Fig. 2 and section 3 of Duarte et al. (2017) and in the Supporting information
179 file. These data sets include wind speed, air temperature, precipitation, and specific humidity (Hudson et al., 2015); incident
180 surface short and longwave radiation (Hudson et al., 2016); ice temperature and salinity (Gerland et al., 2017); sea surface
181 current velocity, temperature, salinity and heat fluxes from a turbulence instrument cluster (TIC) (Peterson et al., 2016); sea
182 surface nutrient concentrations (Assmy et al., 2016) and sea ice biogeochemistry (Assmy et al., 2017). Ocean forcing is based
183 on measurements within the surface 2 meters which provide the boundary condition for the sea ice model. Model forcing files
184 may be found in Duarte (2021c).

185 Refrozen lead simulations started with zero ice, whereas Second Year Ice Simulations started with initial conditions described
186 in the Supporting information file (Table S3).

187 We ran simulations with the standard formulations for biogeochemical processes described in Jeffery et al. (2016) and settings
188 described in Duarte et al. (2017), using mushy thermodynamics, vertically resolved biogeochemistry, and including: freezing,
189 flushing, brine mixed length and molecular diffusion within the ice and at the interface between the ocean and the sea ice as

190 nutrient exchange mechanisms (Jeffery et al., 2011, 2016). We contrasted the above simulations against others that replaced
191 brine molecular and mixed length diffusion of nutrients at the interface between the ocean and the sea ice with diffusion driven
192 by current velocity shear (Table 1), calculated similar to heat exchanges, and following the parameterization described in
193 McPhee et al. (2008) and detailed above (equations 2 - 7). This contrast provides insight into the effects of velocity shear on
194 nutrient diffusion, ice algal production ($\text{mg C m}^{-2} \text{ d}^{-1}$), chlorophyll standing stocks ($\text{mg Chl } a \text{ m}^{-2}$) and vertical distribution of
195 chlorophyll concentration ($\text{mg Chl } a \text{ m}^{-3}$) [note that CICE model output for algal biomass in mmol N m^{-3} was converted to mg
196 $\text{Chl } a \text{ m}^{-3}$ as in Duarte et al. (2017), using $2.1 \text{ mg Chl } a \text{ mmol N}^{-1}$ and following Smith et al. (1993)]. However, due to the
197 concurrent effects of algal biomass exchange between the ocean and ice, such a contrast is not enough to explicitly test our
198 hypothesis and conclude about the effects of turbulent-driven nutrient supply on ice algal nutrient limitation. Therefore,
199 simulations were also run contrasting the same model setups, as described above, but restarting from similar algal standing
200 stocks and vertical distributions within the ice and, switching off algal inputs from the water to the ice. This was done by
201 nullifying the variable algalN, defining the ocean surface background ice algal concentration, in file icepack_zbgc.F90,
202 subroutine icepack_init_ocean_bio and in the restart files. In the case of the RL simulations that started with zero ice, first a
203 simulation was run until the 12 May, and then the obtained ice conditions were used to restart new simulations without algal
204 inputs from the ocean ($\text{algalN} = 0 \text{ mmol N m}^{-3}$). This way, when the simulations restarted, there was already an ice algal
205 standing stock necessary for the modelling experiments developed herein. The SYI simulations were, by default, “restart
206 simulations”, beginning with observed ice physical and biogeochemical variables. Therefore, there was already an algal
207 standing stock in the ice from the onset (Text S1 and Table S3).

208 McPhee et al. (2008) estimated different values for α_s depending on whether the sea ice is growing (highest value) or melting
209 (lowest value) (Table 1). When running simulations for the RL, in some cases, we used only the minimum or the maximum
210 values for α_s to allow for a more extreme contrast between molecular and turbulent diffusion parameterizations. This was done
211 since the former value will tend to minimize differences, whereas the latter will tend to emphasize them. We also completed
212 simulations for the RL and for SYI changing between the maximum and the minimum values of α_s , when ice was growing or
213 melting, respectively, and following McPhee et al. (2008) (see Table 1 for details). This parameterization with a variable α_s
214 is likely the most realistic one, accounting for double diffusion during ice melting (McPhee et al., 2008).

215 Apart from contrasting the way bottom-ice exchanges of nutrients were calculated, some simulations contrasted different
216 parameters related to silicate limitation (Table 1). This approach follows Duarte et al. (2017), where simulations were tuned
217 by changing the Si:N ratio and the half saturation constant for silicate uptake because silicate limitation was leading to an
218 underestimation of algal growth. From this exercise we were able to assess if such tuning was still necessary after implementing
219 turbulent diffusion at the interface between the ocean and the sea ice, driven by velocity shear. Moreover, we repeated
220 simulations with varying snow heights to further investigate the interplay between light and nutrient limitation under
221 contrasting nutrient diffusion parameterizations (Table 1).

222

223

224

225

226

227

228

229

230

231

232 **Table 1. Model simulations.** Refrozen lead (RL) simulation RL_Sim1 corresponds to RL_Sim5 described in Duarte et al. (2017) - the simulation leading
 233 to a best fit to the observations in that study. The remaining RL simulations 2 – 5 differ from RL_Sim1 in using turbulent diffusion at the interface between
 234 the ocean and the sea ice for nutrients in a comparable way as it is calculated for heat and driven by velocity shear. Moreover, RL_Sim5 differs in the
 235 concentration of ice algae in the water column that colonize the sea ice bottom (algalN) and in silicate limitation related parameters. These changes were
 236 done iteratively to fit the model to the observations. In RL_Sim2 and RL_Sim3 the maximum ($\alpha_s=0.006$) and the minimum ($\alpha_s=0.006/70=8.6 \cdot 10^{-5}$) values
 237 recommended by McPhee et al. (2008), respectively, are used throughout the simulations, to provide extreme case scenarios for comparison with RL_Sim1.
 238 In RL_Sim4, $\alpha_s=8.6 \cdot 10^{-5}$ when ice is not growing and 0.006 otherwise, as recommended by McPhee et al. (2008), to account for double diffusive processes
 239 during ice melting that slow down mass exchanges. The remaining RL simulations (RL_Sim6-9) are like the previous ones (RL_Sim1-4, respectively),
 240 except for algalN that was set to zero mmol N m^{-3} , and all simulations were restarted with the same values for all variables. Therefore, simulations 6 – 9
 241 may differ only from 13 May 2015, when they were restarted. Second year ice simulation SYI_Sim_1 is based on Duarte et al. (2017) SYI_Sim4 but without
 242 algal motion. SYI_Sim2 and SYI_Sim3 use turbulent diffusion at the interface between the ocean and the sea ice. The former uses a decreased half
 243 saturation constant for silicate uptake, just like SYI_Sim1, whereas the latter uses the standard CICE value. The remaining SYI simulations (SYI_Sim4
 244 and 5) are like SYI_Sim1 and 2, except for algalN that was set to zero. Simulations SYI_Sim1 and SYI_Sim2 were repeated but with different initial snow
 245 thickness of 30, 20 and 15 cm to further investigate the interplay between light and silicate limitation (see text). Modified parameter values from one
 246 simulation to the next are marked in bold, separately for RL and SYI simulations. Modified parameters are based on literature ranges [e.g. Brzezinski
 247 (1985) and Heggseth (1992), for ratio_Si2N_diatoms, Nelson and Treguer (1992), for K_Sil_diatoms], Urrego-Blanco et al. (2016), for R_snow], or on
 248 previous model calibration work (Duarte et al., 2017). Parameters values were modified in the model input file ice_in, except for algalN and α_s , that are
 249 hard-coded.

Simulations	Modified parameters (bold types below indicate the parameter abbreviation used in Icepack)					
	Silica to nitrogen ratio in diatoms (ratio_Si2N_diatoms)	Half saturation constant for silicate uptake (K_Sil_diatoms, mM Si)	Ice algal concentration in the water (algalN, mM N)	Boolean to define the usage of either molecular (0) or turbulent diffusion (1) (Bottom_turb_mi x)	Interface salt/nutrient turbulent exchange coefficient (α_s)	Sigma coefficient for snow grain (R_snow)
RL_Sim1	1.0	2.2	$11 \cdot 10^{-4}$	0	-	1.5
RL_Sim2	1.0	2.2	$11 \cdot 10^{-4}$	1	0.006	1.5
RL_Sim3	1.0	2.2	$11 \cdot 10^{-4}$	1	8.6 \cdot 10^{-5}	1.5
RL_Sim4	1.0	2.2	$11 \cdot 10^{-4}$	1	8.6 \cdot 10^{-5}-0.006	1.5
RL_Sim5	1.7	5.0	$4 \cdot 10^{-4}$	1	$8.6 \cdot 10^{-5}-0.006$	1.5
RL_Sim6-9	As RL_Sim1-RL_Sim4, respectively		0	As RL_Sim1-RL_Sim4, respectively		
SYI_Sim1	1.0	2.2	$11 \cdot 10^{-4}$	0	-	0.8

SYI_Sim2	1.0	2.2	$11 \cdot 10^{-4}$	1	$8.6 \cdot 10^{-5}$-0.006	0.8
SYI_Sim3	1.0	4.0	$11 \cdot 10^{-4}$	1	$8.6 \cdot 10^{-5}$ -0.006	0.8
SYI_Sim4 and 5	As SYI_Sim1 and SYI_Sim2, respectively		0		As SYI_Sim1 and SYI_Sim2, respectively	

250

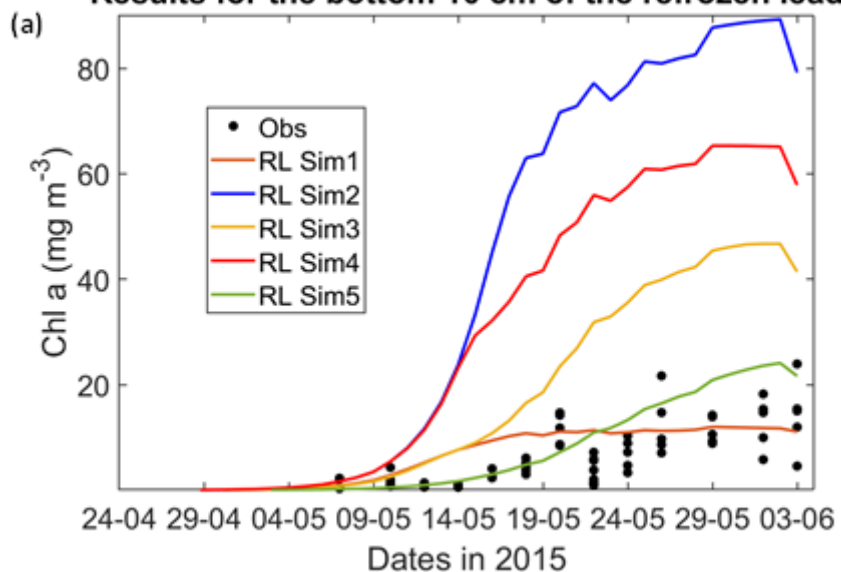
252 3. Results

253 The results of the simulations listed in Table 1 and presented below may be found in Duarte (2021d).

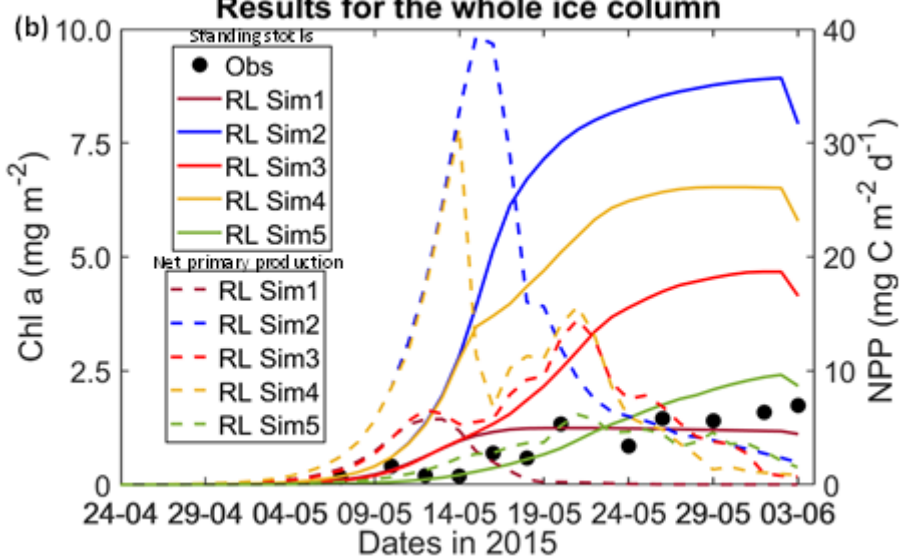
254 3.1 Refrozen lead simulations

255 All simulations with turbulent diffusion (RL_Sim2 – RL_Sim5, Table 1), predict higher bottom chlorophyll *a* (*Chl a*)
256 concentration than with the standard molecular diffusion formulation (RL_Sim1) (Fig. 1a). Simulations RL_Sim2 - 4 grossly
257 overestimate observations. Simulation RL_Sim3, using the lowest value for α_s , is closer both to observations and to RL_Sim1,
258 as well as RL_Sim5, with the latter having the same α_s values of RL_Sim4 but a half saturation constant for silicate limitation
259 increased from its tuned value in Duarte et al. (2017) of 2.2 μM to 5.0 μM and algalN reduced (Table 1) to bring model results
260 closer to observations. Patterns between simulations for the whole ice column and considering both standing stocks and net
261 primary production, are similar to those observed for the bottom-ice (Fig. 1b). Algal biomass is concentrated at the bottom
262 layers (Fig. 2). Concentrations in the layers located between the bottom and the top of the biogrid, defined by the vertical
263 extent (brine height) of the brine network (green lines in the map plots) (Jeffery et al., 2011) are $< 10 \text{ mg Chl } a \text{ m}^{-3}$. Ice
264 thickness, temperature and salinity profiles are extremely similar among these simulations (Figs. S1 and S2).265 Results for the silicate and nitrogen limiting factors are based on brine concentrations. Limiting factors exhibiting lower values
266 (more limitation) in RL simulations are silicate, followed by light (Figs. 3, S3 – S5). Limiting values for silicate range between
267 zero (maximum limitation) and one (no limitation), with stronger limitation after May 13 in all simulations (Fig. 3). The most
268 severe silicate limitation is for RL_Sim1, where values drop to near zero around middle May. Despite the high average bottom
269 *Chl a* concentration predicted in all simulations the bottom layer is where silicate limitation is less severe after May 13. This
270 is more evident in simulations with turbulent bottom diffusion, where light limitation at the bottom-ice becomes more severe
271 than silicate limitation around the end of May (Fig. S6).272 Results obtained with RL_Sim6-9, without algal exchanges between the ocean and the ice (see Table 1), show similar patterns
273 of those observed with RL_Sim1-5, respectively (Fig. 4 versus Fig. 2, Fig. S9 versus Fig. 3, Figs. S7 and S8 versus Figs. S1
274 and S2, Figs. S10 – S12 versus Figs. S3 – S5).275 Interface diffusivity (one of CICE diagnostic variables, corresponding to the diffusion coefficient between adjacent
276 biogeochemical layers and between the bottom layers and the ocean) for simulations with turbulent exchanges ($\alpha_{su} * H$) are up
277 to two orders of magnitude higher at the bottom (diffusivity between the bottom layer and the ocean) than for the RL_Sim1
278 simulation with only molecular diffusion (D_m) + the mixed length diffusion coefficient (D_{MLD}) (refer 2.1 and Fig. 5).

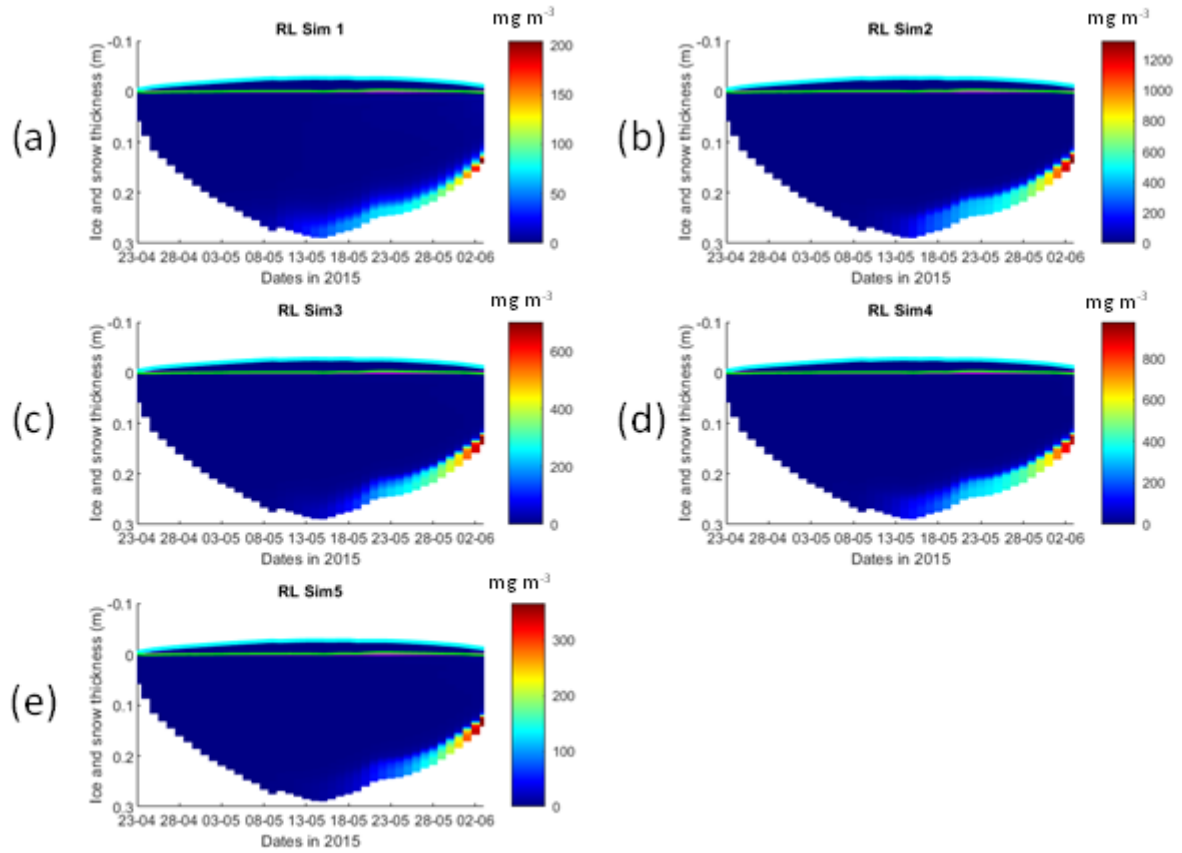
Results for the bottom 10 cm of the refrozen lead



Results for the whole ice column

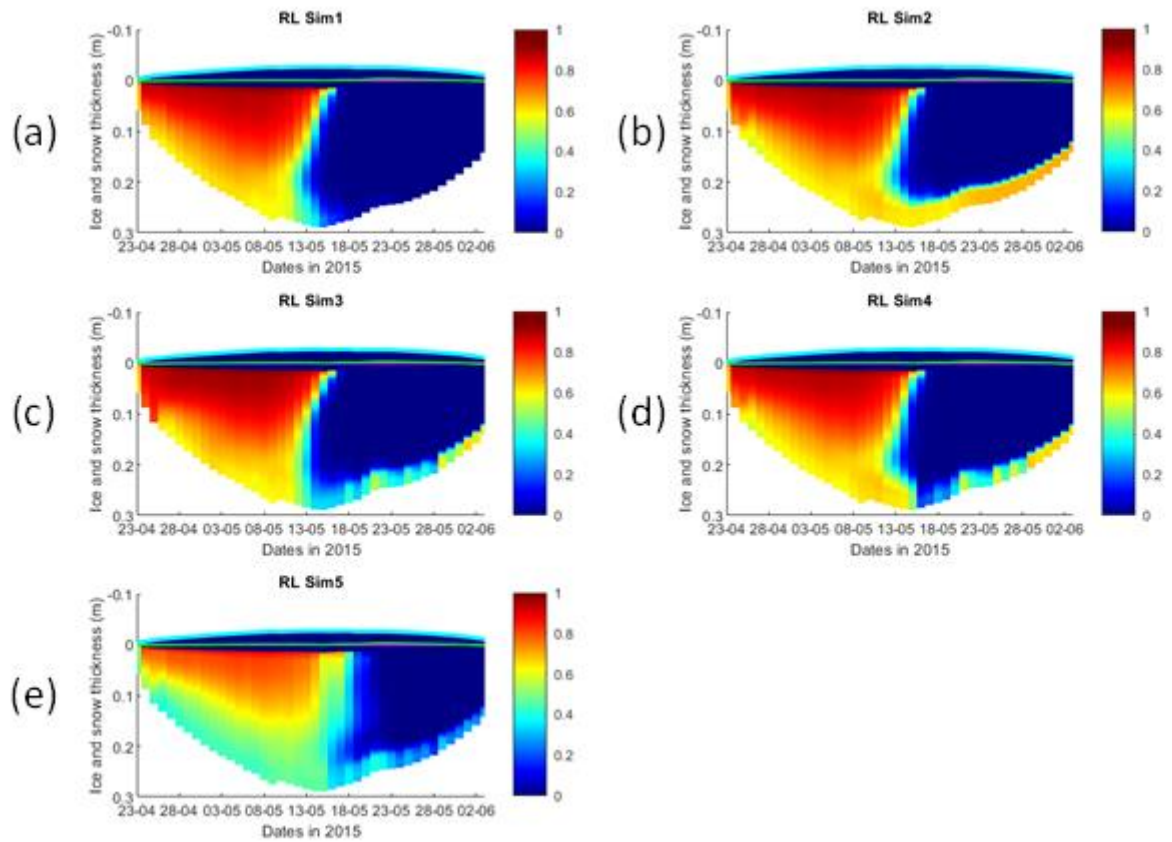


280
281 Figure 1. Daily averaged results for the refrozen lead (RL): (a) Observed and modelled *Chl a* concentration values averaged for the
282 ice bottom 10 cm; (b) Observed and modelled *Chl a* standing stock (continuous lines) and modelled net primary production (NPP)
283 (dashed lines) for the whole ice column (refer to Table 1 for details about model simulations). Observations are the same presented
284 in Duarte et al. (2017).



285

286 **Figure 2. Daily averaged results for the refrozen lead (RL) simulations 1 - 5: Simulated evolution of ice algae *Chl a* as a function of**
 287 **time and depth in the ice (note the colour scale differences between the various panels). Ice thickness is given by the distance between**
 288 **the upper and the lower limits of the maps. The upper regions of the graphs, above the green line with zero values, are above the**
 289 **CICE biogrid and have no brine network. The magenta line, partly covered by the green line, represents sea level. Refer to Table 1**
 290 **for details about model simulations.**



291

292

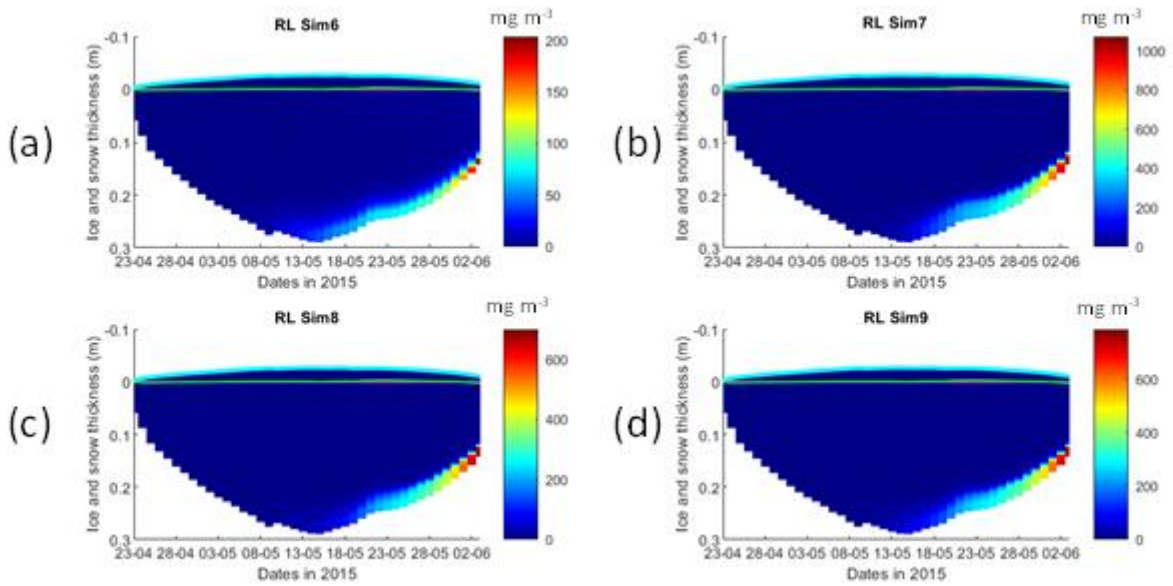
293

294

295

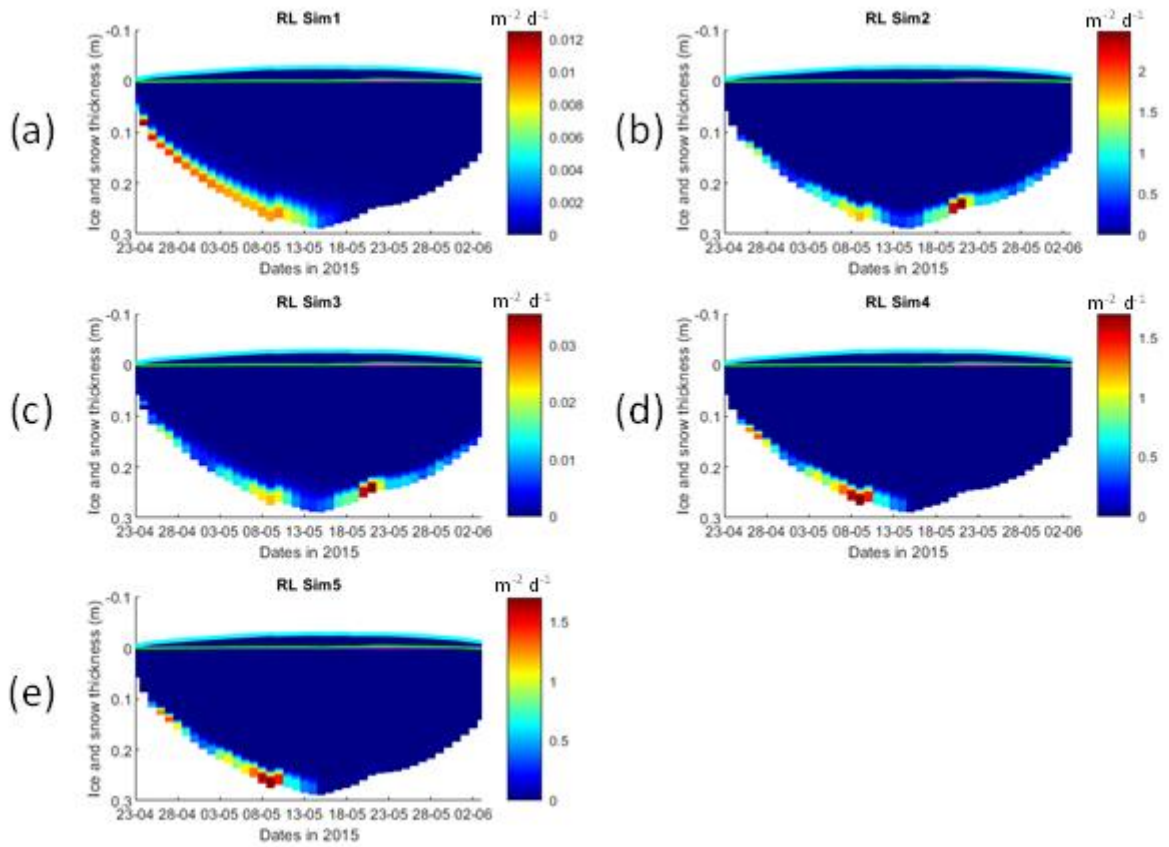
296

Figure 3. Daily averaged results for the refrozen lead (RL) simulations 1 - 5: Simulated evolution of silicate limitation (one means no limitation and zero is maximal limitation), as a function of time and depth in the ice. Ice thickness is given by the distance between the upper and the lower limits of the maps. The upper regions of the graphs, above the green line with zero values, are above the CICE biogrid and have no brine network. The magenta line, partly covered by the green line, represents sea level. Refer to Table 1 for details about model simulations.



297

298 **Figure 4. Daily averaged results for the refrozen lead (RL) simulations 6 - 9: Simulated evolution of ice algae *Chl a* as a function of**
 299 **time and depth in the ice (note the colour scale differences between the various panels). Ice thickness is given by the distance**
 300 **between the upper and the lower limits of the maps. The upper regions of the graphs, above the green line with zero values,**
 301 **are above the CICE biogrid and have no brine network. The magenta line, partly covered by the green line, represents sea level. Refer to Table 1**
 302 **for details about model simulations.**



303

304 **Figure 5. Daily averaged results for the refrozen lead (RL) simulations 1-5: Simulated evolution of interface diffusivity as a function**
 305 **of time and depth in the ice (note the colour scale differences between the various panels). Ice thickness is given by the distance**
 306 **between the upper and the lower limits of the maps. The upper regions of the graphs, above the green line with zero values, are**
 307 **above the CICE biogrid and have no brine network. The magenta line represents sea level. Refer to Table 1 for details about model**
 308 **simulations.**

309

310 3.2 Second year ice simulations

311 Simulations with turbulent diffusion (SYI_Sim2 and 3), predict only slightly higher standing stocks and net primary production
 312 than with the standard molecular diffusion formulation (SYI_Sim1) (Fig. 6). The visual fit to the standing stock observations
 313 is comparable between the various simulations. Changing the half saturation constant for silicate limitation from 2.2 to 4.0 μM
 314 has no impact on model results. This is confirmed by analysing the evolution of *Chl a* concentration as a function of time and
 315 depth in the ice (Fig. 7), with only minor differences being apparent towards the end of the simulation, when *Chl a* increases

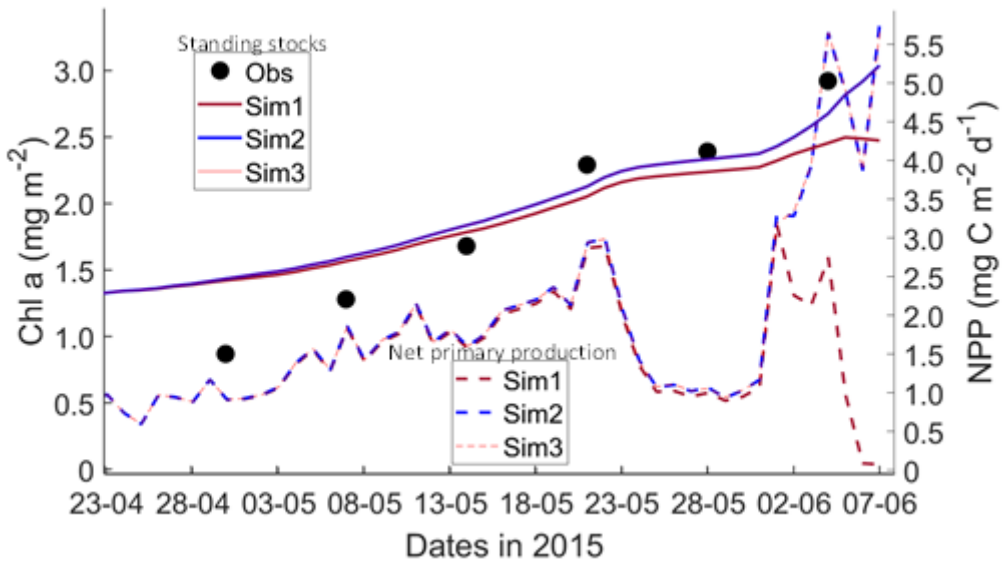
316 at the bottom layers in the simulations with turbulent diffusion (SYI_Sim 2 and 3). Ice thickness, temperature and salinity
317 profiles are extremely similar among these simulations (Fig. S13).

318 The dominant limiting factor in these simulations is light, followed by silicate (compare Fig. 8a, c and e with 8b, d and f and
319 with Fig. S14). Light limitation is less severe after the onset of snow and ice melting at the beginning of June. Silicate limitation
320 is very strong above the bottom ice. Nitrogen limitation is highest at a depth range between ~0.4 ~0.7 m below the ice top,
321 with a large overlap with the depth range where a *Chl a* maximum is observed (Fig. 7). Maximal *Chl a* concentration predicted
322 for the RL_Sim1 and RL_Sim5 simulations - those closer to observations - are two orders of magnitude higher than those
323 predicted for SYI (Fig. 2a and e versus Fig. 7). However, standing stocks predicted for RL_Sim1 and RL_Sim5 simulations
324 are smaller than for SYI simulations, as confirmed by the observations (Figs. 1b and 6). Opposite to what was described for
325 the RL simulations, silicate limitation becomes more severe than light limitation at the bottom layer only in SYI_Sim_1, at the
326 beginning of June, close to the end of the simulation (Fig. S15).

327 Results obtained without algal exchanges between the ocean and the ice (SYI_Sim4 and 5, see Table 1), show the same patterns
328 of those observed with SYI_Sim1 and 2, respectively (Fig. 9 versus Fig. 7, Fig. S17 versus Fig. 8, Figs. S18 versus S14a - d
329 and Figs. S16 versus S13a - d).

330 Interface diffusivity (one of CICE diagnostic variables, see above) for simulations with turbulent bottom exchanges are up to
331 four orders of magnitude higher at the bottom ice than for simulations with only molecular diffusion (Fig. S19, showing a
332 comparison between SYI_Sim1 and SYI_Sim2).

333 SYI_Sim1 and 2 were repeated with varying snow thickness (Table 1 and Figs. 10 and 11). In the former simulation (Fig. 10a),
334 as snow height decreases, there is a reduction in light limitation and a sharp increase in silicate limitation, overtaking light
335 limitation (values becoming lower) as early as mid-May. In the latter simulation (Fig. 10b), light limitation prevails irrespective
336 of snow height, except in the case of the lower snow height of 15 cm where silicate becomes more limiting towards the end of
337 the simulation. With the decrease in snow height, there is an increase in *Chl a* concentration in all simulations. Highest values
338 for SYI_Sim2 are ~one order of magnitude larger than those for SYI_Sim1. Moreover, the decrease in snow heights is followed
339 by an earlier and more intense bottom ice algal bloom.



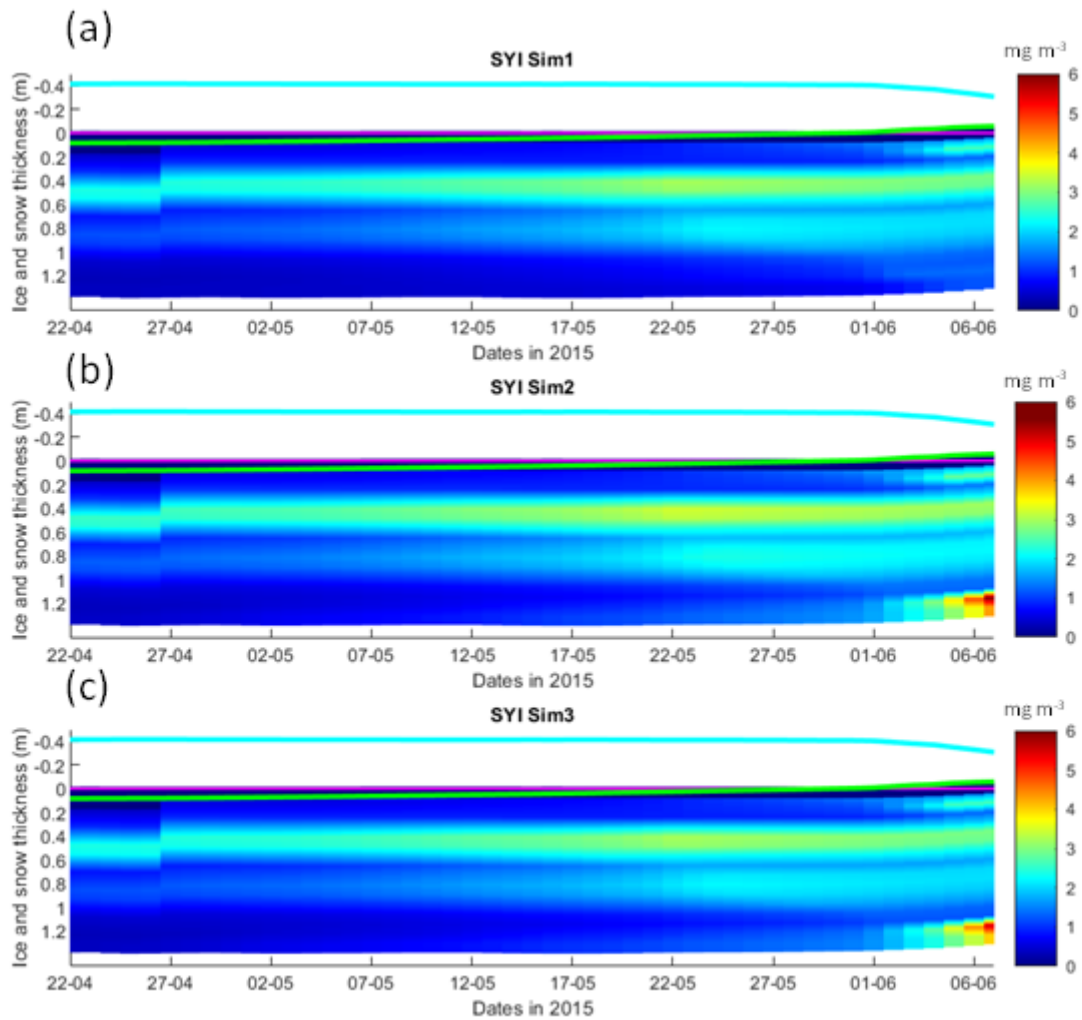
340

341

342

343

Figure 6. Daily averaged results for second year ice (SYI) simulations 1 - 3: Observed [same data presented in Duarte et al. (2017)] and modelled $Chl\alpha$ standing stock (continuous lines) and modelled net primary production (NPP) (dashed lines) for the whole ice column (refer to Table 1 for details about model simulations).



344

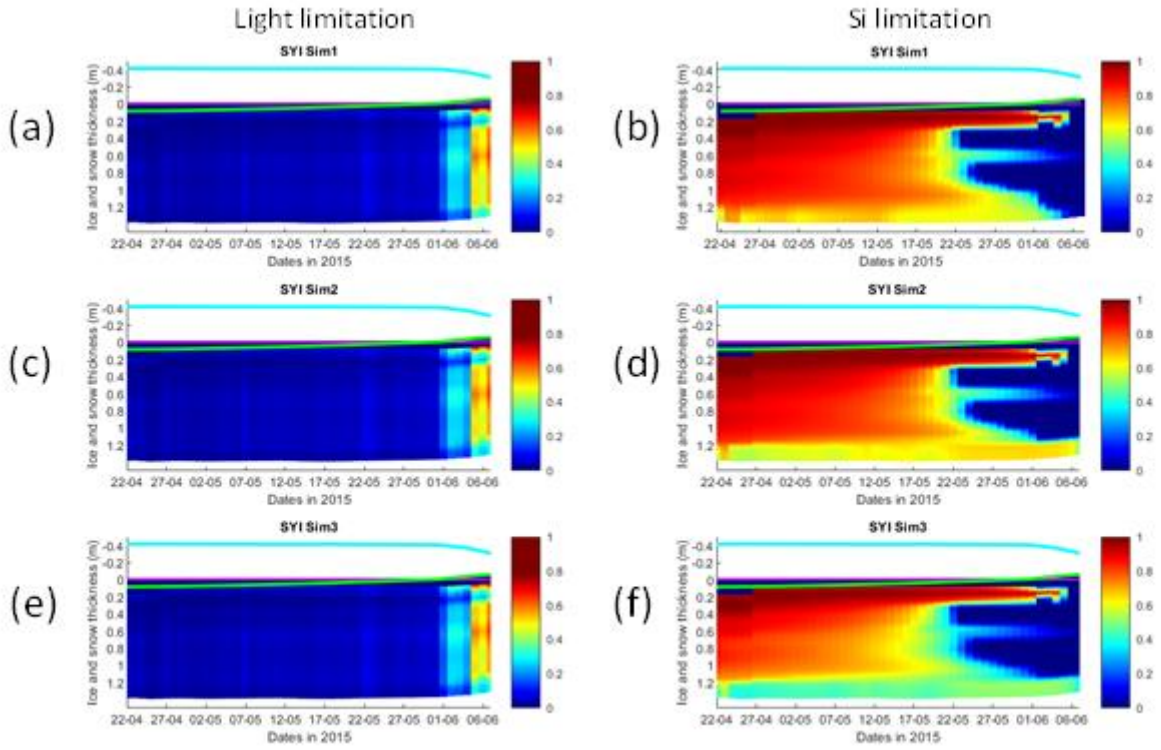
345

346

347

348

Figure 7. Daily averaged results for second year ice (SYI) simulations 1 - 3: Simulated evolution of ice algae *Chl a* as a function of time and depth in the ice. The upper regions of the graphs, above the green line with zero values, are above the CICE biogrid and have no brine network. The magenta line represents sea level, and the cyan line represents the top of the snow layer. Refer to Table 1 for details about model simulations.



349

350

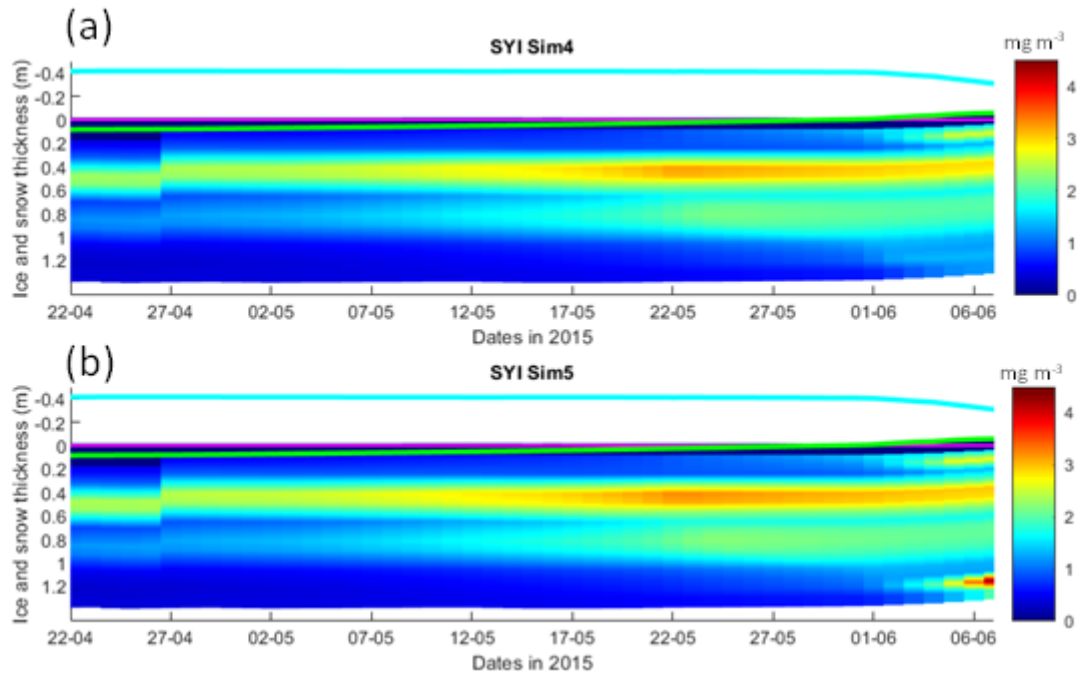
351

352

353

354

Figure 8. Daily averaged results for second year ice (SYI) simulations 1 - 3: Simulated evolution of light (left panels) and silicate (right panels) limitation (one means no limitation and zero is maximal limitation), as a function of time and depth in the ice. The upper regions of the graphs, above the green line with zero values, are above the CICE biogrid and have no brine network. The magenta line represents sea level, and the cyan line represents the top of the snow layer. Refer to Table 1 for details about model simulations.



355

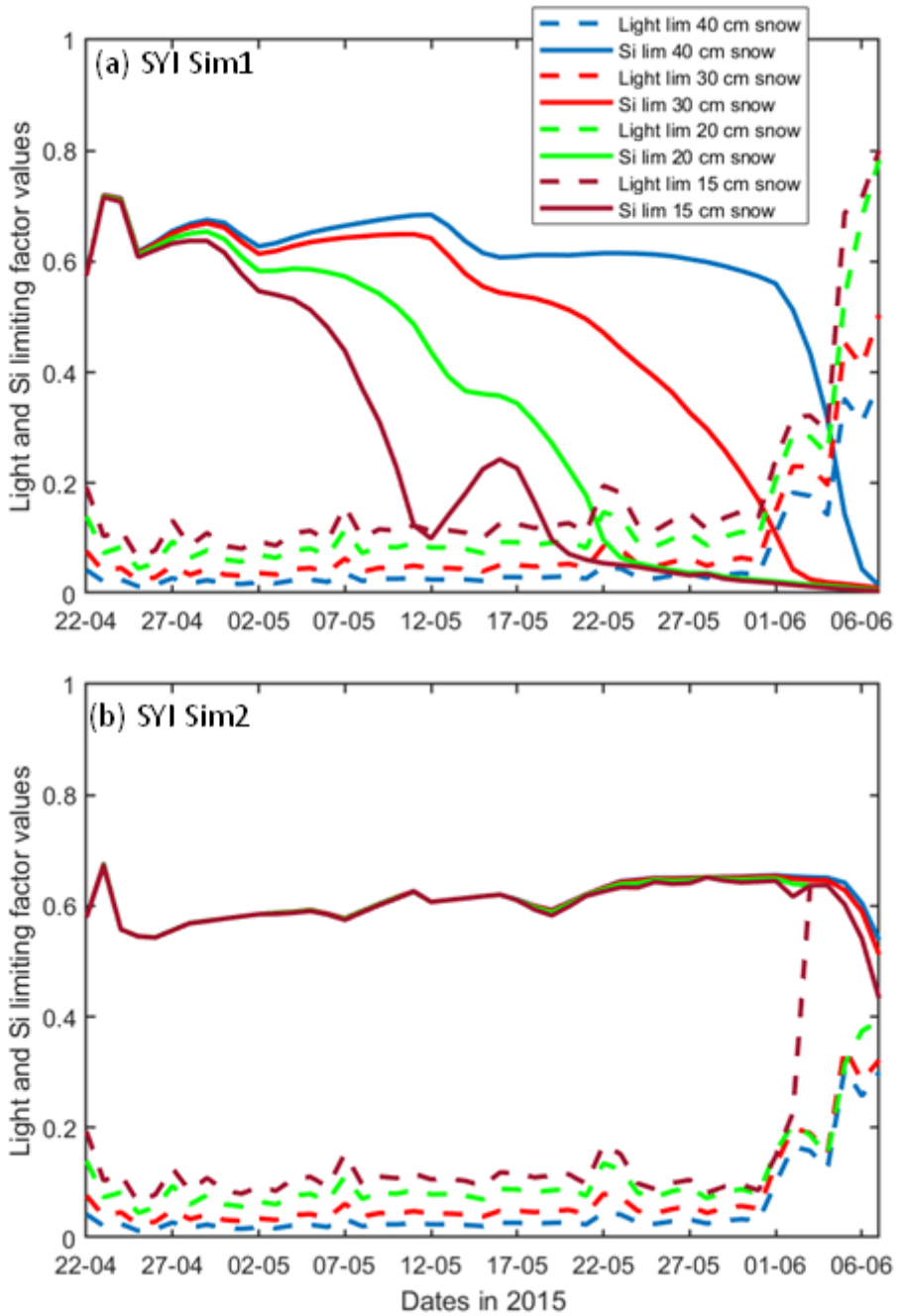
356

357

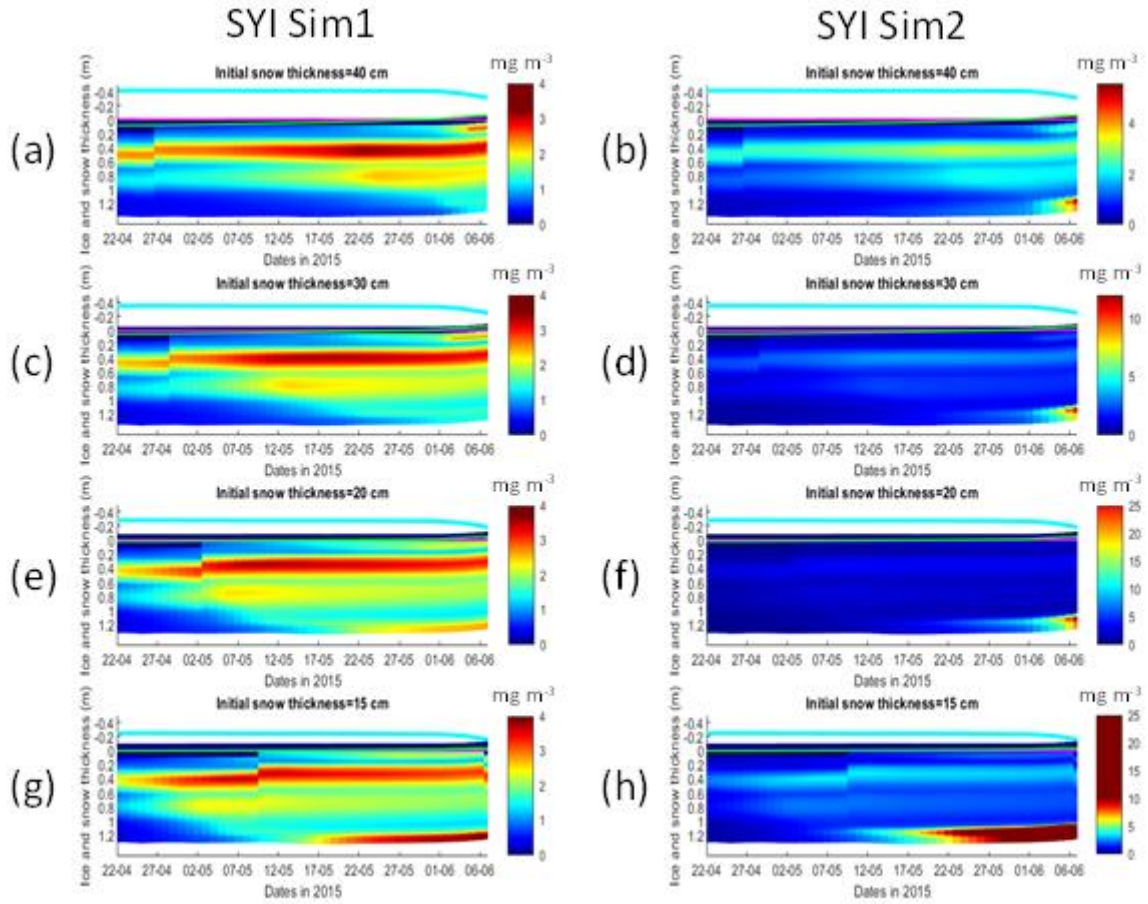
358

359

Figure 9. Daily averaged results for second year ice (SYI) simulations 4 and 5: Simulated evolution of ice algae *Chl a* as a function of time and depth in the ice. The upper regions of the graphs, above the green line with zero values, are above the CICE biogrid and have no brine network. The magenta line represents sea level, and the cyan line represents the top of the snow layer. Refer to Table 1 for details about model simulations.



360
361 **Figure 10.** Daily averaged results for the second-year ice (SYI) simulations 1 (a) and 2 (b) starting with a snow depth of 40 (default
362 simulation), 30, 20 and 15 cm: Simulated evolution of light (dashed lines) and silicate (continuous lines) limitation (one means no
363 limitation and zero is maximal limitation), as a function of time at the ice bottom layer (one means no limitation). Refer to Table 1
364 for details about model simulations.



365
366
367
368
369
370

Figure 11. Daily averaged results for second year ice (SYI) simulations 1 (left panels) and 2 (right panels) starting with a snow depth of 40 (default simulation), 30, 20 and 15 cm: Simulated evolution of ice algae *Chl a* as a function of time and depth in the ice. The upper regions of the graphs, above the green line with zero values, are above the CICE biogrid and have no brine network. The magenta line represents sea level, and the cyan line represents the top of the snow layer. Refer to Table 1 for a description of model simulations.

371 **4. Discussion**

372 The results obtained in this study support the initial hypothesis, showing that considering the role of velocity shear on turbulent
373 nutrient exchanges between the ocean and the sea ice, formulated in a way consistent with heat exchanges, leads to a reduction
374 in nutrient limitation that supports a significant increase in ice algal net primary production and *Chl a* biomass accumulation
375 in the bottom ice layers, when production is nutrient limited. Therefore, our results are in line with empirical evidence provided
376 by Cota et al. (1987) and Dalman et al. (2019) but, to the best of our knowledge, experimental evidence from properly designed
377 experiments is still lacking to test our hypothesis. Moreover, our results do not imply necessarily that experiments carried out

378 with other sea-ice models would render the same trends. The implementation of turbulent mixing considerably relieved silicate
379 limitation in the RL simulations, leading to an increase in NPP, in the duration of the algal growth period, in bottom *Chl a*
380 concentration and in-ice light absorption, increasing light limitation due to shelf-shading [in the CICE model, optical ice
381 properties are influenced by ice algal concentrations (Jeffery et al., 2016)].

382 In the N-ICE2015 biogeochemical dataset (Assmy et al., 2016), the median of dissolved inorganic nitrogen to silicate ratios in
383 all surface and subsurface water masses, is above 1.7 (unpublished data), which is the upper limit for the nitrogen to silicate
384 ratio for polar diatoms (e.g. Takeda, 1998; Krause et al. 2018). Therefore, it can be expected that, in the region covered by the
385 N-ICE2015 expedition, silicate is more limiting than nitrogen for the production yields of the pennate diatoms characteristic
386 of the bottom-ice communities [the dominant algal functional group in bottom ice, e.g. Leu et al. (2015), van Leeuwe et al.
387 (2019)]. Elsewhere in the Arctic the opposite may be true, considering nitrate and silicate concentrations presented in Leu et
388 al. (2015) and the number of process studies documenting such limitation [e.g., Campbell et al. (2016)]. However, the
389 conclusions taken here about the effects of turbulent mixing are independent of the limiting nutrient.

390 Implementing turbulent diffusion between the ice and the ocean has obvious implications for model tuning. Our results for the
391 RL show that with this formulation it was necessary to increase the half saturation constant for silicate uptake and to reduce
392 the ocean concentration of algal nitrogen (algalN), reducing the colonization of bottom ice by ice algae, to obtain *Chl a* values
393 comparable to those observed (RL_Sim5). Therefore, whereas Duarte et al. (2017) had to reduce silicate limitation to improve
394 the fit between modelled and observational data, the opposite approach was required when using turbulent diffusion in line
395 with results reported in Lim et al. (2019) for Antarctic sea ice diatoms. This is an example of how one can get good model
396 results by the wrong reasons with difficult to predict consequences on model forecasts under various scenarios.

397 In the SYI case, only a minor increase in bottom *Chl a* concentration was observed towards the end of simulations SYI_Sim_2
398 and SYI_Sim_3, when light limitation due to the thick snow cover was relieved by snow melt. Silicate limitation was not as
399 severe as in SYI_Sim_1, due to greater bottom exchanges in the former simulations. The importance of snow cover in
400 controlling ice algal phenology has been stressed before [e.g., Campbell et al. (2015), Leu et al. (2015)].

401 Duarte et al. (2017) used the delta-Eddington parameter, corresponding to the standard deviation of the snow grain size
402 (R_{snow}) (Urrego-Blanco et al., 2016), to tune model predicted shortwave radiation at the ice bottom. However, there was
403 still a positive shortwave model bias in June. Therefore, our conclusion about the main limiting role of light in SYI is
404 conservative. Moreover, in part of SYI cores sampled during the N-ICE2015 expedition, in the period covered by our
405 simulations, with an unusually high snow thickness (~40 cm), there was no *Chl a* bottom maximum (Duarte et al., 2017; Olsen
406 et al., 2017).

407 The dominant role of light limitation in SYI was confirmed in the simulations with reduced snow thickness and alleviated light
408 limitation, with a bottom-ice algal *Chl a* maximum emerging earlier at snow thickness ≤ 20 cm. The reduction of snow
409 thickness had a much larger effect in increasing *Chl a* concentration at the bottom layer when turbulent mixing was used, due
410 to lower silicate limitation. Reducing snow thickness led to a relatively early shift from light to silicate limitation when we
411 used molecular and mixed length diffusion, whereas this shift occurred only at the very end of the simulated period when we

412 used turbulent diffusion at the ice-ocean interface, driven by velocity shear, instead of molecular diffusion. The effects of
413 different types of diffusion, upon reduction of the snow cover and the possible development of a bottom ice algal bloom, are
414 critical aspects when simulating ice algal phenology and attempting to quantify the contribution of sea ice algae to Arctic
415 primary production.

416 Simulated shear-driven turbulent diffusivities are up to four orders of magnitude higher than molecular + mixed length
417 diffusivities at the bottom ice and the results presented herein emphasize their potential role in sea ice biogeochemistry. The
418 number and intensity of Arctic winter storms has increased over the 1979–2016 period (Rinke et al., 2017; Graham et al.,
419 2017) and the effect of more frequent and more intensive winter storms in the Atlantic Sector of the Arctic Ocean is a thinner,
420 weaker, and younger snow-laden ice pack (Graham et al., 2019). Storms that occur late in the winter season, after a deep
421 snowpack has accumulated, have the potential to promote ice growth by dynamically opening leads where new ice growth can
422 take place. The young ice of the refrozen leads does not have time to accumulate a deep snow layer until the melting season,
423 which could lead to light limitation of algal growth. All things considered, it can be expected that ongoing trends in the Arctic
424 will lead to a release from light limitation in increasingly larger areas of the ice pack in late winter, which will lead to more
425 likely nutrient limitation earlier in spring (e.g. Lannuzel et al. 2020). These effects will be further amplified under thinning of
426 the snowpack as observed in western Arctic, and in the Beaufort and Chukchi seas, over the last decades (Webster et al., 2014).
427 Therefore, properly parameterizing nutrient exchanges between the ice and the ocean in sea-ice biogeochemical models is of
428 utmost importance to avoid overestimating nutrient limitation and thus underestimating sea ice algal primary production.

429 In existing sea-ice models there are “natural” differences between the way budgets for non-conservative tracers such as
430 nutrients are closed compared to those of heat and salt, which are related to the biogeochemical sinks and sources (e.g., equation
431 18 in Vancoppenolle et al., 2010), but also some “inconsistencies”, related with the way their transfers between the ocean and
432 the ice are computed. Interestingly, some models (e.g., Jin et al., 2006, 2008 and Hunke et al., 2016) apply the diffusion
433 equation to calculate exchanges across the bottom ice not only to dissolved tracers, but also to algal cells. This is to guarantee
434 a mechanism of ice colonization by microalgae. However, the usage of the same coefficient for dissolved and particulate
435 components creates significant uncertainty.

436 Molecular diffusion is a slow process compared with turbulent exchanges. This justifies the usage of diffusion coefficients
437 which are much higher than molecular diffusivity, as in Jin et al. (2006), using a value of $1.0 \cdot 10^{-5} \text{ m}^2 \text{ s}^{-1}$, four orders of
438 magnitude higher than the value indicated in Mann and Lazier (2005) – $1.5 \cdot 10^{-9} \text{ m}^2 \text{ s}^{-1}$ – or the parameterization of molecular
439 diffusivity as a function of friction velocity as in Mortenson et al. (2017). The approach proposed herein, formulating bottom-
440 ice nutrient exchanges in a way that is consistent with heat exchanges, provides a physically sound, consistent, and easy to
441 implement alternative.

442 Calculating diffusion fluxes across the molecular sublayer may be challenging, since it is necessary to estimate the boundary
443 concentrations of this layer, which is only a few tenths of millimetre thick (e.g. Lavoie et al., 2005). This implies resolving
444 with a great detail the ocean surface layer (*sensu* MacPhee, 2008), which is not practical with standalone sea ice models but
445 doable with coupled ocean-sea ice models. Moreover, one needs to know whether exchanges of heat, salt and nutrients are

446 dominated by molecular exchange or by turbulent exchange. This may be challenging on its own since it depends not only on
447 knowing friction velocities but also on knowing the roughness of the bottom ice (e.g. Olsen et al.2019). Ideally, when using
448 coupled ocean-sea ice models, and assuming it is practical to estimate the type of dominant exchanges, one may use either the
449 approach described by Lavoie et al. (2005) or the approach described herein based on McPhee (2008) and grounded on
450 experimental work. Whatever the case, it seems rather likely that we still lack the measurements to properly evaluate these
451 various approaches and find an optimal solution. The way forward implies the availability of eddy covariance data for 3D
452 current velocity, temperature, salinity and ideally, a limiting nutrient, collected at the sea ice-ocean interface over periods of
453 sea ice growth and melting. Such data should be accompanied by vertical profiles for the same tracers, at high resolution,
454 across the surface and the mixing layers (*sensu* McPhee, 2008) and by sea ice bottom samples. Such experiments may be
455 carried out in the sea and in sea ice laboratories under controlled conditions, and they will help to evaluate the results presented
456 herein and improving the parameterizations used in models for the sea ice-ocean interface. Another layer of complexity are
457 the effects of sea ice ridges and keels on the turbulent exchange coefficients (Tsamados et al., 2014). According to these
458 authors such effects are important for regional sea ice modelling, which reinforces the need of experimental studies of the type
459 mentioned above.

460 5. Conclusions

461 Considering the role of velocity shear on turbulent nutrient exchanges at the interface between the ocean and the ice in a sea-
462 ice biogeochemical sub-model, leads to a reduction in nutrient limitation and a significant increase in ice algal net primary
463 production and *Chl a* biomass accumulation in the bottom-ice layers, when production is nutrient limited. The results presented
464 herein emphasize the potential role of bottom-ice nutrient exchange processes, irrespective of brine dynamics and other
465 physical-chemical processes, in delivering nutrients to bottom-ice algal communities, and thus the importance of properly
466 including them in sea-ice models. The relevance of this becomes even more apparent considering ongoing changes in the
467 Arctic icescape, with a predictable decrease in light limitation as ice becomes thinner and more fractured, with an expected
468 reduction in snow cover.

469 Code availability

470 The software code used in this study may be found at:

471 <https://doi.org/10.5281/zenodo.4675097> and <https://doi.org/10.5281/zenodo.5795034>.

472 This code is in a fork derived from the CICE Consortium repository (<https://github.com/CICE-Consortium>).

473 The Consortium's codes are open-source with a standard 3-clause BSD license and are is under the following Copyright
474 license, available at (<https://cice-consortium-cice.readthedocs.io/en/master/intro/copyright.html>)

476 **Data availability**
477 Model forcing function files may be found at: <https://doi.org/10.5281/zenodo.4672176>
478 Results from model simulations described above, in the form of CICE daily netCDF history files iceh.* may be found at:
479 <http://doi.org/10.5281/zenodo.4672210>
480 There is one directory for each simulation, and it includes besides the historical files the input file (ice_in) with the simulation
481 parameters.
482
483 **Authors contribution**
484 Pedro Duarte made the software changes, designed the experiments, performed the simulations and prepared the manuscript
485 with contributions from all co-authors.
486 Philipp Assmy contributed to the writing of the manuscript.
487 Karley Campbell contributed to the writing of the manuscript.
488 Arild Sundfjord contributed to the writing of the manuscript and to funding acquisition.
489
490 **Competing interests**
491 The authors declare that they have no conflict of interest.
492
493 **Acknowledgements**
494 This work has been supported by the Fram Centre Arctic Ocean flagship project “Mesoscale physical and biogeochemical
495 modelling of the ocean and sea-ice in the Arctic Ocean” (project reference 66200), the Norwegian Metacenter for
496 Computational Science application “NN9300K - Ecosystem modelling of the Arctic Ocean around Svalbard”, the Norwegian
497 “Nansen Legacy” project (no. 276730) and the European Union’s Horizon 2020 research and innovation programme under
498 grant agreement No 869154 (project FACE-IT). Contributions by K Campbell are supported by the Diatom ARCTIC project
499 (NE/R012849/1;03F0810A), part of the Changing Arctic Ocean program, jointly funded by the UKRI Natural Environment
Research Council and the German Federal Ministry of Education and Research (BMBF).
500
501 **References**
502 Arrigo, K. R., Kremer, J. N., and Sullivan, C. W.: A Simulated Antarctic Fast Ice Ecosystem, *J. Geophy. Res.*, 98, 17, 1993.
503 Assmy, P., Duarte, P., Dujardin, J., Fernández-Méndez, M., Fransson, A., Hodgson, R., Kauko, H., Kristiansen, S., Mundy, C.
504 J., Olsen, L. M., Peeken, I., Sandbu, M., Wallenschus, J., Wold, A.: N-ICE2015 water column biogeochemistry [Data set],
Norwegian Polar Institute, <https://doi.org/10.21334/npolar.2016.3ebb7f64>, 2017.

505 Assmy, P., Dodd, P. A., Duarte, P., Dujardin, J., Elliott, A., Fernández-Méndez, M., Fransson, A., Granskog, M. A., Hendry,
506 K., Hodgson, R., Kauko, H., Kristiansen, S., Leng, M. J., Meyer, A., Mundy, C. J., Olsen, L. M., Peeken, I., Sandbu, M.,
507 Wallenschus, J., Wold, A.: N-ICE2015 sea ice biogeochemistry [Data set], Norwegian Polar Institute,
508 <https://doi.org/10.21334/npolar.2017.d3e93b31>, 2017.

509 Brzezinski, M. A.: The Si-C-N Ratio of Marine Diatoms - Interspecific Variability and the Effect of Some Environmental
510 Variables, *J. Phycol.*, 21, 347-357, 1985.

511 Campbell, K., Mundy, C. J., Barber, D. G. and Gosselin, M.: Characterizing the sea ice algae chlorophyll a-snow depth
512 relationship over Arctic spring melt using transmitted irradiance, *J. Mar. Sys.*, 147, 76-84, doi:
513 <https://doi.org/10.1016/j.jmarsys.2014.01.008>, 2015.

514 Campbell, K., Mundy, C. J., Landy, J. C., Delaforge, A., Michel, C. and Rysgaard, S.: Community dynamics of bottom-ice
515 algae in Dease Strait of the Canadian Arctic. *Prog. Oceanogr.*, 149, 27-39, doi: <http://dx.doi.org/10.1016/j.pocean.2016.10.005>,
516 2016.

517 Carmack, E.: Circulation and Mixing in Ice-Covered Waters, in: *The Geophysics of Sea Ice*. NATO ASI Series (Series B:
518 Physics), edited by Untersteiner N. Springer, Boston, MA. 641-712, https://doi.org/10.1007/978-1-4899-5352-0_11, 1986.

519 Cota, G. F., Prinsenberg, S. J., Bennett, E. B., Loder, J. W., Lewis, M. R., Anning, J. L., Watson, N. H. F., and Harris, L. R.:
520 Nutrient Fluxes during Extended Blooms of Arctic Ice Algae, *J. Geophys. Res.-Oceans*, 92, 1951-1962, doi:
521 10.1029/Jc092ic02p01951, 1987.

522 Cota, G. F., and Horne, E. P. W.: Physical Control of Arctic Ice Algal Production, *Mar. Ecol. Prog. Ser.*, 52, 111-121, doi:
523 10.3354/meps052111, 1989.

524 Cota, G. F., and Sullivan, C. W.: Photoadaptation, Growth and Production of Bottom Ice Algae in the Antarctic, *J. Phycol.*,
525 26, 399-411, doi: 10.1111/j.0022-3646.1990.00399.x, 1990.

526 Dalman, L. A., Else, B. G. T., Barber, D., Carmack, E., Williams, W. J., Campbell, K. , Duke, P. J., Kirillov, S., and Mundy,
527 C. J.: Enhanced bottom-ice algal biomass across a tidal strait in the Kitikmeot Sea of the Canadian Arctic, *Elem. Sci. Anth.*, 7,
528 doi: <https://doi.org/10.1525/elementa.361>, 2019.

529 Duarte, P., Meyer, A., Olsen, L. M., Kauko, H. M., Assmy, P., Rosel, A., Itkin, P., Hudson, S. R., Granskog, M. A., Gerland,
530 S., Sundfjord, A., Steen, H., Hop, H., Cohen, L., Peterson, A. K., Jeffery, N., Elliott, S. M., Hunke, E. C., and Turner, A. K.:
531 Sea ice thermohaline dynamics and biogeochemistry in the Arctic Ocean: Empirical and model results, *J. Geophys. Res.-*
532 *Biogeosciences*, 122, 1632-1654, doi: 10.1002/2016JG003660, 2017.

533 Duarte, P.: CICE-Consortium/Icepack: Icepack with bottom drag, heat and nutrient turbulent diffusion (Version 1.1). Zenodo.
534 [\(2021a, April 9\).](http://doi.org/10.5281/zenodo.4675021)

535 Duarte, P.: CICE-Consortium/CICE: CICE with bottom drag, heat and nutrient turbulent diffusion (Version 1.1). Zenodo.
536 [\(2021b, April 9\).](http://doi.org/10.5281/zenodo.4675097)

537 Duarte, P.: The importance of turbulent ocean-sea ice nutrient exchanges for simulation of ice algal biomass and production
538 with CICE6.1 and Icepack 1.2 - CICE forcing files (Version v1.0) [Data set]. Zenodo. <http://doi.org/10.5281/zenodo.4672176>,
539 2021c.

540 Duarte, P.: The importance of turbulent ocean-sea ice nutrient exchanges for simulation of ice algal biomass and production
541 with CICE6.1 and Icepack 1.2 - model simulations (Version v1.0) [Data set]. Zenodo. <http://doi.org/10.5281/zenodo.4672210>,
542 2021c.

543 Gerland, S., Granskog, M. A., King, J, Rösel, A.: N-ICE2015 Ice core physics: temperature, salinity and density [Data set],
544 Norwegian Polar Institute, <https://doi.org/10.21334/npolar.2017.c3db82e3>, 2017.

545 Gosselin, M., Legendre, L., Demers, S., and Ingram, R. G.: Responses of Sea-Ice Microalgae to Climatic and Fortnightly Tidal
546 Energy Inputs (Manitounuk Sound, Hudson-Bay), *Can. J. Fish. Aquat. Sci.*, 42, 999-1006, doi: 10.1139/f85-125, 1985.

547 Graham, R. M., Rinke, A., Cohen, L., Hudson, S. R., Walden, V. P., Granskog, M. A., Dorn, W., Kayser, M., and Maturilli,
548 M.: A comparison of the two Arctic atmospheric winter states observed during N-ICE2015 and SHEBA, *J. Geophys. Res.-*
549 *Atmospheres*, 122, 5716-5737, doi: 10.1002/2016JD025475, 2017.

550 Graham, R. M., Itkin, P., Meyer, A., Sundfjord, A., Spreen, G., Smedsrud, L. H., Liston, G. E., Cheng, B., Cohen, L., Divine,
551 D., Fer, I., Fransson, A., Gerland, S., Haapala, J., Hudson, S. R., Johansson, A. M., King, J., Merkouriadi, I., Peterson, A. K.,
552 Provost, C., Randelhoff, A., Rinke, A., Rosel, A., Sennechael, N., Walden, V., Duarte, P., Assmy, P., Steen, H., and Granskog,
553 M. A.: Winter storms accelerate the demise of sea ice in the Atlantic sector of the Arctic Ocean, *Sci. Rep.-Uk*, 9, Artn 9222,
554 doi: 10.1038/S41598-019-45574-5, 2019.

555 Granskog, M. A., Fer, I., Rinke, A., and Steen, H.: Atmosphere-Ice-Ocean-Ecosystem Processes in a Thinner Arctic Sea Ice
556 Regime: The Norwegian Young Sea ICE (N-ICE2015) Expedition, *J. Geophys. Res.-Oceans*, 123, 1586-1594, doi:
557 10.1002/2017jc013328, 2018.

558 Hegseth, E. N.: Sub-Ice Algal Assemblages of the Barents Sea - Species Composition, Chemical-Composition, and Growth-
559 Rates, *Polar. Biol.*, 12, 485-496, 1992.

560 Hudson, S. R., Cohen, L., Walden, V.: N-ICE2015 surface meteorology [Data set], Norwegian Polar Institute,
561 <https://doi.org/10.21334/npolar.2015.056a61d1>, 2015.

562 Hudson, S. R., Cohen, L., Walden, V.: N-ICE2015 surface broadband radiation data [Data set], Norwegian Polar Institute,
563 <https://doi.org/10.21334/npolar.2016.a89cb766>, 2016.

564 Hunke, E. C., Lipscomb, W. H., Turner, A. K., Jeffery, N., Elliot, S.: CICE: the Los Alamos Sea Ice Model. Documentation
565 and User's Manual Version 5.1. Los Alamos National Laboratory, USA. LA-CC-06-012, 2015.

566 Ingram, R. G., Osler, J. C., and Legendre, L.: Influence of Internal Wave-Induced Vertical Mixing on Ice Algal Production in
567 a Highly Stratified Sound, *Estuar. Coast. Shelf. S.*, 29, 435-446, doi: 10.1016/0272-7714(89)90078-4, 1989.

568 Jeffery, N., Hunke, E. C., and Elliott, S. M.: Modeling the transport of passive tracers in sea ice, *J. Geophys. Res.-Oceans*,
569 116, Artn C07020, doi:10.1029/2010jc006527, 2011.

570 Jeffery, N., Elliott, S., Hunke, E. C., Lipscomb, W. H., Turner, A. K.: Biogeochemistry of CICE: The Los Alamos Sea Ice
571 Model, Documentation and User's Manual. Zbgc_colpkg modifications to Version 5, Los Alamos National Laboratory, Los
572 Alamos, N. M., 2016.

573 Jin, M., Deal, C. J., Wang, J., Shin, K. H., Tanaka, N., Whitledge, T. E., Lee, S. H., and Gradinger, R. R.: Controls of the
574 landfast ice–ocean ecosystem offshore Barrow, Alaska, *Ann. Glaciol.*, 44, 9, 2006.

575 Jin, M., Deal, C., and Jia, W.: A coupled ice-ocean ecosystem model for I-D and 3-D applications in the Bering and Chukchi
576 Seas, *Chinese Journal of Polar Science*, 19, 11, 2008.

577 Krause, J. W., Duarte, C. M., Marquez, I. A., Assmy, P., Fernandez-Mendez, M., Wiedmann, I., Wassmann, P., Kristiansen,
578 S., and Agusti, S.: Biogenic silica production and diatom dynamics in the Svalbard region during spring, *Biogeosciences*, 15,
579 6503-6517, doi: 10.5194/bg-15-6503-2018, 2018.

580 Lake, R. A, Lewis, E. L.: Salt rejection by sea ice during growth, *J. Geophys. Res.*, 75, 583-597, 1970.

581 Lannuzel, D., Tedesco, T., van Leeuwe, M., Campbell, K., Flores, H., Delille, B., Miller, L., Stefels, J., Assmy, P., Bowman,
582 J., Brown, K., Castellani, G., Chierici, M., Crabeck, O., Damm, E., Else, B., Fransson, A., Fripiat, F., Geilfus, N. X., Jacques,
583 C., Jones, E., Kaartokallio, H., Kotovitch, M., Meiners, K., Moreau, S., Nomura, D., Peeken, I., Rintala, J. M., Steiner, N.,
584 Tison, J. L., Vancoppenolle, M., Van der Linden, F., Vichi, M. and Wongpan, P.: The future of Arctic sea-ice biogeochemistry
585 and ice-associated ecosystems, *Nat. Clim. Change* 10(11), 983-992, doi: <https://doi.org/10.1038/s41558-020-00940-4>, 2020.

586 Lavoie, D., Denman, K., and Michel, C.: Modeling ice algal growth and decline in a seasonally ice-covered region of the
587 Arctic (Resolute Passage, Canadian Archipelago), *J. Geophys. Res.-Oceans*, 110, Artn C11009, doi: 10.1029/2005jc002922,
588 2005.

589 Leu, E., Mundy, C. J., Assmy, P., Campbell, K., Gabrielsen, T. M., Gosselin, M., Juul-Pedersen, T., and Gradinger, R.: Arctic
590 spring awakening - Steering principles behind the phenology of vernal ice algal blooms, *Progr. Oceanogr.*, 139, 151-170, doi:
591 10.1016/j.pocean.2015.07.012, 2015.

592 Lim, S. M., Moreau, S., Vancoppenolle, M., Deman, F., Roukaerts, A., Meiners, K. M., Janssens, J., and Lannuzel, D.: Field
593 Observations and Physical-Biogeochemical Modeling Suggest Low Silicon Affinity for Antarctic Fast Ice Diatoms, *J Geophys
594 Res-Oceans*, 124, 7837-7853, 10.1029/2018jc014458, 2019.

595 Mann, K. H., Lazier, J. R. N.: *Dynamics of Marine Ecosystems*, Third Edition, Blackwell Publishing Ltd., Carlton, Victoria
596 3053, Australia, 503p., doi:10.1002/9781118687901, 2005.

597 McPhee, M.: Air-ice-ocean interaction: Turbulent ocean boundary layer exchange processes. Springer-Verlag, New York,
598 216p., doi: 10.1007/978-0-387-78335-2, 2008.

599 McPhee, M. G., Morison, J. H., and Nilsen, F.: Revisiting heat and salt exchange at the ice-ocean interface: Ocean flux and
600 modeling considerations, *J. Geophys. Res.-Oceans*, 113, Artn C06014, doi: 10.1029/2007jc004383, 2008.

601 Mortenson, E., Hayashida, H., Steiner, N., Monahan, A., Blais, M., Gale, M. A., Galindo, V., Gosselin, M., Hu, X. M., Lavoie,
602 D., and Mundy, C. J.: A model-based analysis of physical and biological controls on ice algal and pelagic primary production
603 in Resolute Passage, *Elem. Sci. Anth.*, 5, Artn 39, doi:10.1525/elementa.229, 2017.

604 Nelson, D. M., and Treguer, P.: Role of Silicon as a Limiting Nutrient to Antarctic Diatoms - Evidence from Kinetic-Studies
605 in the Ross Sea Ice-Edge Zone, *Mar. Ecol. Prog. Ser.*, 80, 255-264, doi: 10.3354/meps080255, 1992.

606 Niedrauer, T. M., and Martin, S.: Experimental-Study of Brine Drainage and Convection in Young Sea Ice, *J. Geophys. Res.-*
607 *Oceans*, 84, 1176-1186, doi: 10.1029/JC084iC03p01176, 1979.

608 Notz, D., and Worster, M. G.: Desalination processes of sea ice revisited, *J Geophys Res-Oceans*, 114, Artn C05006, doi:
609 10.1029/2008jc004885, 2009.

610 Olsen, L. M., Laney, S. R., Duarte, P., Kauko, H. M., Fernández-Méndez, M., Mundy, C. J., Rösel, A., Meyer, A., Itkin, P.,
611 Cohen, L., Peeken, I., Tatarek, A., Różańska, M., Wiktor, J., Taskjelle, T., Pavlov, A. K., Hudson, S. R., Granskog, M. A.,
612 Hop, H., and Assmy, P.: The seeding of ice-algal blooms in Arctic pack ice: the multiyear ice seed repository hypothesis, *J*
613 *Geophys Res-Biogeosciences*, 122(7), 1529-1548, doi: 10.1002/2016jg003668, 2017.

614 Olsen, L. M., Duarte, P., Peralta-Ferriz, C., Kauko, H. M., Johansson, M., Peeken, I., Różańska-Pluta, M., Tatarek, A., Wiktor,
615 J., Fernández-Méndez, M., Wagner, P. M., Pavlov, A. K., Hop, H., and Assmy, P.: A red tide in the pack ice of the Arctic
616 Ocean, *Sci Rep*, 9, 9536, 10.1038/s41598-019-45935-0, 2019.

617 Peterson, A. K., Fer, I., Randelhoff, A., Meyer, A., Håvik, L., Smedsrød, L. H., Onarheim, L., Muilwijk, M., Sundfjord, A.,
618 McPhee, M. G.: N-ICE2015 Ocean turbulent fluxes from under-ice turbulence cluster (TIC) [Data set], Norwegian Polar
619 Institute, <https://doi.org/10.21334/npolar.2016.ab29f1e2>, 2016.

620 Reeburgh, W. S.: Fluxes Associated with Brine Motion in Growing Sea Ice, *Polar Biol.*, 3, 29-33, doi: 10.1007/Bf00265564,
621 1984.

622 Rinke, A., Maturilli, M., Graham, R. M., Matthes, H., Handorf, D., Cohen, L., Hudson, S. R., and Moore, J. C.: Extreme
623 cyclone events in the Arctic: Wintertime variability and trends, *Environ. Res. Letters*, 12, Artn 094006, doi:10.1088/1748-
624 9326/Aa7def, 2017.

625 Smith, R. E. H., Cavaletto, J. F., Eadie, B. J., and Gardner, W. S.: Growth and Lipid-Composition of High Arctic Ice Algae
626 during the Spring Bloom at Resolute, Northwest-Territories, Canada, *Mar. Ecol. Prog. Ser.*, 97, 19-29, doi:
627 10.3354/meps097019, 1993.

628 Takeda, S.: Influence of iron availability on nutrient consumption ratio of diatoms in oceanic waters, *Nature*, 393, 774-777,
629 doi: 10.1038/31674, 1998.

630 Tedesco, L., Vichi, M.: BFM-SI: a new implementation of the Biogeochemical Flux Model in sea ice. in: CMCC Research
631 Papers, <http://www.cmcc.it/publications-meetings/publications/researchpapers/rp0081-ans-03-2010>,
632 <http://hdl.handle.net/2122/5956>, 2010.

633 Tedesco, L., Vichi, M., and Scoccimarro, E.: Sea-ice algal phenology in a warmer Arctic, *Sci. Adv.*, 5, ARTN eaav4830, doi:
634 10.1126/sciadv.aav4830, 2019.

635 Thomas, M., Vancoppenolle, M., France, J. L., Sturges, W. T., Bakker, D. C. E., Kaiser, J., and von Glasow, R.: Tracer
636 Measurements in Growing Sea Ice Support Convective Gravity Drainage Parameterizations, *J Geophys Res-Oceans*, 125,
637 ARTN e2019JC015791, doi: 10.1029/2019JC015791, 2020.

638 Tsamados, M., Feltham, D. L., Schroeder, D., Flocco, D., Farrell, S. L., Kurtz, N., Laxon, S. W., and Bacon, S.: Impact of
639 Variable Atmospheric and Oceanic Form Drag on Simulations of Arctic Sea Ice*, *Journal of Physical Oceanography*, 44,
640 1329-1353, 10.1175/Jpo-D-13-0215.1, 2014.

641 Turner, A. K., Hunke, E. C., and Bitz, C. M.: Two modes of sea-ice gravity drainage: A parameterization for large-scale
642 modeling, *J. Geophys. Res.-Oceans*, 118, 2279-2294, doi: 10.1002/jgrc.20171, 2013.

643 Urrego-Blanco, J. R., Urban, N. M., Hunke, E. C., Turner, A. K., and Jeffery, N.: Uncertainty quantification and global
644 sensitivity analysis of the Los Alamos sea ice model, *J. Geophys. Res.-Oceans*, 121, 2709-2732, doi: 10.1002/2015JC011558,
645 2016.

646 Vancoppenolle, M., Bitz, C. M., and Fichefet, T.: Summer landfast sea ice desalination at Point Barrow, Alaska: Modeling
647 and observations, *J. Geophys. Res.-Oceans*, 112, Artn C04022, doi: 10.1029/2006jc003493, 2007.

648 Vancoppenolle, M., Goosse, H., de Montety, A., Fichefet, T., Tremblay, B., and Tison, J. L.: Modeling brine and nutrient
649 dynamics in Antarctic sea ice: The case of dissolved silica, *J Geophys Res-Oceans*, 115, Artn C02005, doi:
650 10.1029/2009jc005369, 2010.

651 Vancoppenolle, M., Bopp, L., Madec, G., Dunne, J., Ilyina, T., Halloran, P. R., and Steiner, N.: Future Arctic Ocean primary
652 productivity from CMIP5 simulations: Uncertain outcome, but consistent mechanisms, *Global Biogeochem Cy*, 27, 605-619,
653 doi: 10.1002/gbc.20055, 2013.

654 van Leeuwe, M. A., Tedesco, L., Arrigo, K. R., Assmy, P., Campbell, K., Meiners, K. M., Rintala, J. M., Selz, V., Thomas,
655 D. N. and Stefels, J.: Microalgal community structure and primary production in Arctic and Antarctic sea ice: A synthesis.
656 *Elem. Sci. Anth.*, 6:4., doi: <https://doi.org/10.1525/elementa.267>, 2018.

657 Wakatsuchi, M., and Ono, N.: Measurements of Salinity and Volume of Brine Excluded from Growing Sea Ice, *J. Geophys.*
658 *Res.-Oceans*, 88, 2943-2951, doi: 10.1029/JC088iC05p02943, 1983.

659 Webster, M. A., Rigor, I. G., Nghiem, S. V., Kurtz, N. T., Farrell, S. L., Perovich, D. K. and Sturm, M.: Interdecadal changes
660 in snow depth on Arctic sea ice, *J. Geophys. Res.-Oceans* 119(8), 5395-5406, doi:10.1002/2014JC009985, 2014.

661 Wells, A. J., Wetlaufer, J. S., and Orszag, S. A.: Brine fluxes from growing sea ice, *Geophys Res Lett*, 38, Artn L04501, doi:
662 10.1029/2010gl046288, 2011.

663

664

665

666

667

668